# Overcoming the Thermal Instability of Efficient Polymer Solar Cells by Employing Novel Fullerene-Based Acceptors

*Chaohong Zhang, Alexander Mumyatov, Stefan Langner, José Darío Perea, Thaer Kassar, Jie Min, Lili Ke, Haiwei Chen, Kirill L. Gerasimov, Denis V. Anokhin, Dimitri A. Ivanov, Tayebeh Ameri, Andreas Osvet, Diana K. Susarova, Tobias Unruh, Ning Li,* Pavel Troshin,* and Christoph J. Brabec**

Extensive research efforts around the world have been devoted to organic photovoltaics (OPV) over the last decade due to their unique advantages for commercial application, such as low cost, light weight, flexibility, and easy manufacture on large-scale.[1–3] By introducing the bulk heterojunction (BHJ)[4,5] structure into OPV devices, tremendous progress has been achieved to boost the power conversion efficiency (PCE) of OPV devices to the 11% regime.[6–9] The most efficient polymer donors, such as poly(benzodithiophene-co-thieno[3,4-b]thiophene) (PBDTTT)-based polymers,[7] diketopyrrolopyrrole-based polymers,[10] and poly[(5,6-difluoro-2,1,3-benzothiadiazol-4,7-diyl)-alt-(3,3‴-di(2-nonyltridecyl)-2,2′;5′,2″;5″,2‴-quaterthiophen-5,5‴-diyl)] (PffBT4T-$C_9C_{13}$),[6] possess bandgaps of 1.40–1.60 eV and achieve the highest performance so far in combination with the commonly used methanofullerene derivatives like phenyl-$C_{61}$-butyric acid methyl ester ([60]PCBM) or [6,6]-phenyl-$C_{71}$-butyric acid methyl ester ([70]PCBM).[11]

Functional fullerenes, on the one hand, can preserve the properties of pristine fullerenes, such as superior electron-transporting ability and high electron affinity. On the other hand, by properly attaching suitable addends, one can manipulate a wide variety of chemical, physical, or thermodynamic properties, such as better solubility in organic solvents, higher lowest unoccupied molecular orbital (LUMO) level, and improved compatibility with organic donors.[12] These advantages endow functional fullerenes with extraordinary capability, acting as unique electron-accepting components in OPV devices.[2,13] Although PCBM is the most prominent acceptor in OPV devices,[5,14] the energy levels of PCBM should be further optimized in order to achieve high open circuit voltage ($V_{OC}$) in combination with the state-of-the-art organic donors.[15] Fullerene derivatives with more suitable electronic levels are expected to reduce the bandgap to $V_{OC}$ loss and approach the theoretical efficiency limit.[13,16] PCBM bisadduct[17] and indene-$C_{60}$ bisadduct[18] made their glory debut for being well compatible with poly(3-hexylthiophene-2,5-diyl) (P3HT) and for achieving promising high $V_{OC}$ and PCE compared to the PCBM-based counterparts. However, resulting from constitutional isomer impurities and inefficient charge generation, fullerene bisadducts failed to produce similarly satisfying performance with the latest outstanding organic donors.[19] Another effective way of increasing the LUMO level of fullerene derivatives is to add an electron-donating group to the fullerene cage.[20] A series of newly developed functional fullerenes have shown higher photovoltaic performance than PCBM resulting from their high-lying LUMO levels. Itoh and co-workers carried out a systematic study on a series of fulleropyrrolidine derivatives, some of which possess higher $V_{OC}$ and efficiency than PCBM when blended with P3HT.[21] Troshin and co-workers reported that solar cells based on the novel pyrrolidinofullerene acceptors exhibited impressively high $V_{OC}$ and promising efficiency in combination with Poly[*N*-9′-heptadecanyl-2,7-carbazole-*alt*-5,5-(4′,7′-di-2-thienyl-2′,1′,3′-benzothiadiazole)] (PCDTBT) and P3HT compared to the PCBM-based references.[22]

As the PCE of OPV devices was improved to over 11%, currently, more research efforts are required to address the long-term stability issue. Many factors may cause degradation

C. Zhang, S. Langner, J. D. Perea, Dr. J. Min, L. Ke, H. Chen, Dr. T. Ameri, Dr. A. Osvet, Dr. N. Li, Prof. C. J. Brabec
Institute of Materials for Electronics and Energy Technology (i-MEET)
Friedrich-Alexander University Erlangen-Nürnberg
Martensstrasse 7, 91058 Erlangen, Germany
E-mail: ning.li@fau.de; christoph.brabec@fau.de

A. Mumyatov, Dr. D. V. Anokhin, Dr. D. K. Susarova, Prof. P. Troshin
Institute for Problems of Chemical Physics of Russian Academy of Sciences
Semenov Prospect 1, Chernogolovka 142432, Russia
E-mail: troshin@icp.ac.ru

T. Kassar, Prof. T. Unruh
Chair for Crystallography and Structure Physics
Friedrich-Alexander University Erlangen- Nürnberg
Staudtstrasse 3, 91058 Erlangen, Germany

K. L. Gerasimov, Dr. D. V. Anokhin, Prof. D. A. Ivanov
Faculty of Fundamental Physical and Chemical Engineering
Moscow State University
GSP-1, 1–51 Leninskie Gory, Moscow 119991, Russia

Prof. D. A. Ivanov
Institut de Sciences des Matériaux de Mullhouse
CNRS UMR 7361
15 Jean Starcky, F-68051 Mulhouse, France

Prof. P. Troshin
Skolkovo Institute of Science and Technology
Skolkovo Innovation Center
Nobel st. 3, Moscow 143026, Russian Federation

Prof. C. J. Brabec
Bavarian Center for Applied Energy Research (ZAE Bayern)
Haberstrasse 2a, 91058 Erlangen, Germany

**DOI: 10.1002/aenm.201601204**

 © 2016 WILEY-VCH Verlag GmbH & Co. KGaA, Weinheim 

of OPV devices, among which light, heat, oxygen, and humidity are the essential factors. While the effect of oxygen and humidity can be suppressed by proper encapsulation, light and accumulated heat from illumination are inherently unavoidable and must be addressed with the highest priority. Thermal stability is of special importance because heat can result in severely deteriorated performance loss in a short time.[13,23,24] Quite some efforts have been devoted to improving the thermal stability and lifetime of OPV devices. Previous research to tackle this challenge focused on chemically locking the fullerenes, typically, by the following three strategies: (1) Adding cross-linkable groups to the donor materials; (2) PCBM based locking strategy; (3) Addition of cross-linkable small molecule additive.[24] Recently, Mynar and co-workers and Yang and co-workers designed new BDT based donors with fullerene-reactive groups, and improved devices thermal stability to some extent.[25] An alternative even more universal strategy is to modify the fullerene-based acceptors. Poly(ethylene glycol) (PEG) capped fullerene PCB-PEG and [6,6]-phenyl-$C_{61}$ butyric acid pentafluorophenyl ester ($PC_{61}BP^F$) were found to stabilize the P3HT:PCBM solar cells by adding 8 wt%.[26] [6,6]-phenyl-$C_{61}$-butyric acid styryl ester and [6,6]-phenyl-$C_{61}$-butyric acid styryl dendron ester were other successful examples, but were only reported for P3HT:PCBM solar cells so far.[27] Durrant and co-workers gained enhanced morphological stability and performance in several PCBM-based systems by light-induced oligomerization.[28] However, PCBM dimerization leads to performance losses and is thus no viable strategy to enhance stability.[29] More recently, Wantz et al. employed cross-linkable small molecule 4,4′-bis(azidomethyl)biphenyl in the active layer to enhance the thermal stability by sacrificing some degree of efficiency.[30] Zhan and co-workers utilized 4,4′-biphenol to stabilize solar cells with 80% efficiency, preserved after annealing at 130 °C for 120 min.[31]

In this study, we demonstrate efficient organic solar cells based on two novel high LUMO/high $V_{OC}$ fullerene derivatives, a pyrrolidinofullerene (PyF5) and a methanofullerene (FAP1). We further demonstrate that miscibility between donor (D) and acceptor (A) is the essential criteria for enhanced stability, almost independent on the crystallinity of the fullerene. As such, PyF5 was chosen as it is significantly less crystalline than PCBM while FAP1 has comparable or even higher crystallinity. The PyF5- and FAP1-based solar cells attain comparable efficiencies to the PCBM-based references due to an impressive high $V_{OC}$. The performance of all solar cells under thermal stress is examined. The PyF5- and FAP1-based solar cells are found to be extremely stable under isothermal annealing at 140 °C in inert atmosphere. The morphological investigations reveal that negligible morphological change happened to PyF5- and FAP1-based composites after annealing, while significant phase separation induced by PCBM aggregation/crystallization is observed for the PCBM-based films. The miscibility between polymers and fullerenes is in-depth investigated and discussed as the major design rule for enhanced stability of OPV devices.

The device architecture of organic solar cells studied in this work is illustrated in **Figure 1**a. Solution-processed ZnO nanoparticles and thermally evaporated molybdenum oxide ($MoO_x$) were employed as electron and hole transporting layer, respectively. The chemical structures of polymer donors and fullerene-based acceptors are summarized in Figure 1b. Two state-of-the-art polymer donors, poly[4,8-bis(5-(2-ethylhexyl)thiophen-2-yl)benzo[1,2-b;4,5-b′] dithiophene-2,6-diyl-alt-(4-(2-ethylhexyl)-3-fluorothieno[3,4-b]thiophene-)-2-carboxylate-2-6-diyl)] (PTB7-Th) and a low bandgap diketopyrrolopyrrole–quinquethiophene alternating copolymer (pDPP5T-2), were used in this study owing to their promising performance and reproducibility for printed OPV devices.[7,9,10] Two novel fullerenes, PyF5 and FAP1, were synthesized according to previous papers.[22]

The thermal behavior of pristine PTB7-Th and fullerene derivatives is summarized in Figure S1 (Supporting Information). No endothermic peak was observed for pristine PTB7-Th between 30 and 300 °C, while the pristine PCBM

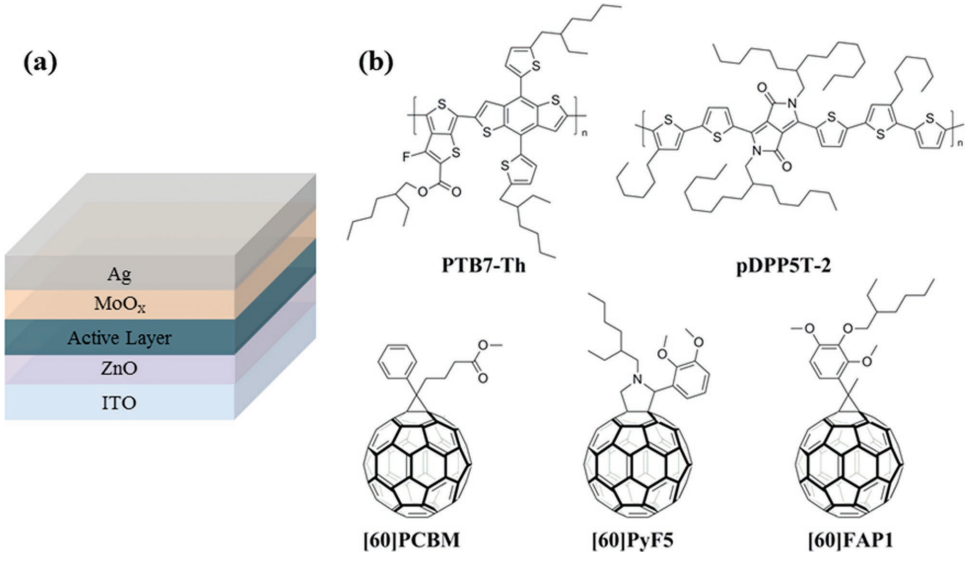


**Figure 1.** a) Schematic device architecture of organic solar cells. b) Chemical structures of donor and acceptor materials.


© 2016 WILEY-VCH Verlag GmbH & Co. KGaA, Weinheim

exhibited melting peak in the first and second heating scans. An exothermic peak at 168 °C was observed during the first heating scan of PCBM, indicating cold crystallization.[32] In contrast to PCBM, during the same temperature range, PyF5 exhibits a broad endothermic feature during the first heating run, implying it being a dominantly amorphous material. This is most likely because PyF5 is a mixture of two stereoisomers due to hindered nitrogen inversion.[22] A melting peak was observed in the first heating scan of pristine FAP1, indicating the crystalline-feature of FAP1. However, no cold crystallization or crystallization was observed in the first heating or first cooling scan for FAP1. Moreover, the glass transition temperature ($T_g$) of pristine PCBM, PyF5, and FAP1 were determined to be 129, 142, and 110 °C, respectively, as shown in Figure S1e (Supporting Information). The crystalline properties of the three fullerenes are further confirmed by grazing-incidence wide-angle X-ray scattering (GIWAXS) data as shown in Figure S2 (Supporting Information). The room-temperature 2D GIWAXS patterns of PCBM reveal two broad reflections of the crystalline phase in addition to the amorphous halo. The reflections likely correspond to poorly organized PCBM crystals. The diffractograms of PyF5 exhibit only amorphous halo. In contrast, the GIWAXS patterns of FAP1 reveal highly oriented narrow peaks of a crystalline phase. Consequently, the degree of ordering in the studied acceptors is different.

The photovoltaic characteristics of PTB7-Th in combination with various fullerene derivatives are summarized in **Figure 2**a and **Table 1**. The external quantum efficiency (EQE) spectra of the corresponding OPV devices are shown in Figure 2b. It is worthwhile to mention that [60]PCBM rather than [70]PCBM was used for the reference devices to guarantee direct comparability with the two $C_{60}$-based fullerenes derivatives. According to literature, the performance of our PTB7-Th:PCBM control device is comparable to the control device processed under similar conditions.[7] The solar cells based on PTB7-Th:PyF5 attained an average PCE of 6.4% along with an enhanced $V_{OC}$ of 0.84 V, which is significantly higher than that (0.78 V) of the PTB7-Th:PCBM control devices. The higher $V_{OC}$ observed in the PyF5-based solar cells is consistent with the higher LUMO of PyF5.[22] PTB7-Th:FAP1 solar cells display an average PCE of 6.0% and again a significantly higher $V_{OC}$ of 0.87 V, indicating that the bandgap to voltage loss is minimized by replacing PCBM with either of the two novel fullerene derivatives. As shown in Figure 2c and Table S1 (Supporting Information), excellent thermal stability was found for the PyF5- and FAP1-based solar cells. The PTB7-Th:PCBM control devices showed rapidly decreased photovoltaic performance upon annealing and maintained only 19% of initial performance after baking at 140 °C for 24 h, while the photovoltaic performance of PyF5- and FAP1-based devices remained almost unchanged under the same conditions. A more detailed investigation on thermal behavior of

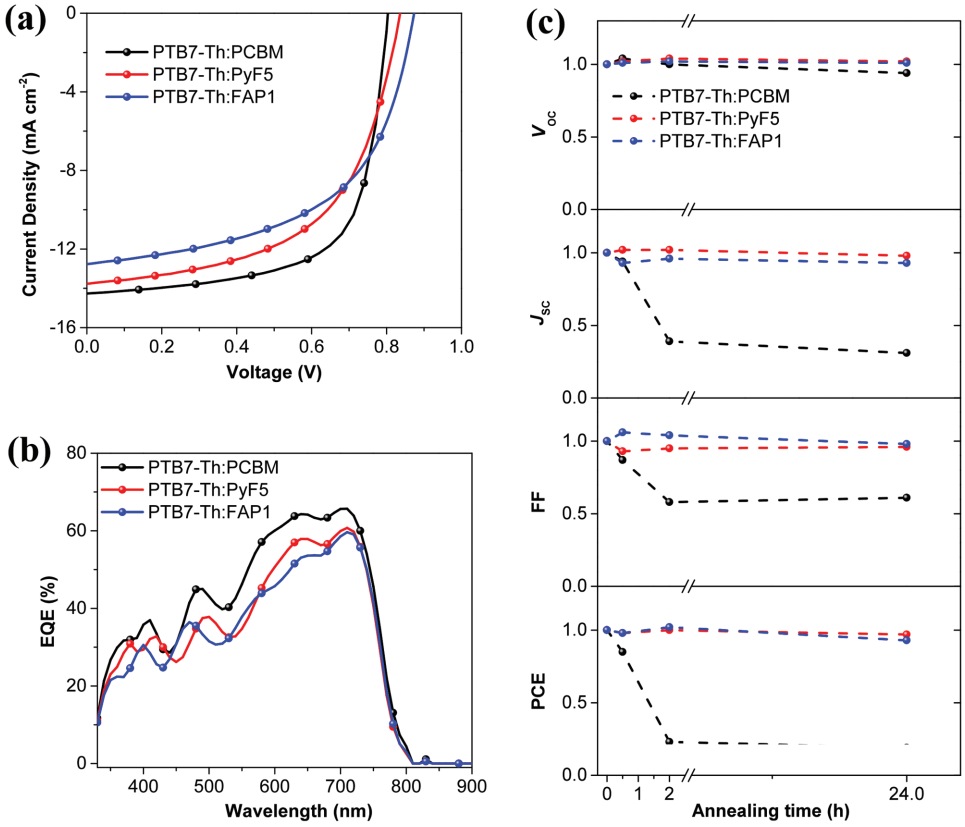


**Figure 2.** a) Current density–voltage (*J*–*V*) curves and b) EQE spectra of PTB7-Th:fullerene solar cells under illumination of AM 1.5 (100 mW cm$^{-2}$). c) Normalized photovoltaic performance of PTB7-Th:fullerene organic solar cells as a function of annealing time at 140 °C under inert atmosphere (all the devices were annealed prior to the deposition of top electrode).


© 2016 WILEY-VCH Verlag GmbH & Co. KGaA, Weinheim

**Table 1.** Photovoltaic characteristics of PTB7-Th based organic solar cells.

| Active layer | D:A wt ratios | $V_{OC}$ [V] | $J_{SC}$ [mA cm$^{-2}$] | FF [%] | PCE [%] | PCE[a)] [%] |
|---|---|---|---|---|---|---|
| PTB7-Th:PCBM | 1:1.5 | 0.78 ± 0.01 | 14.4 ± 1.4 | 65 ± 1.0 | 7.3 ± 0.6 | 19 |
| PTB7-Th:PyF5 | 1:2 | 0.84 ± 0.01 | 13.8 ± 1.2 | 56 ± 0.6 | 6.4 ± 0.5 | 97 |
| PTB7-Th:FAP1 | 1:2 | 0.87 ± 0.01 | 12.6 ± 0.5 | 55 ± 0.4 | 6.0 ± 0.3 | 93 |

[a)]Maintained PCE of OPV devices after annealing at 140 °C for 24 h under inert atmosphere. Values are taken from Figure 2c.

PTB7-Th in combination with various acceptors under different testing conditions are summarized and discussed in the Supporting Information (Figure S3 and Table S2–S4).

As shown in Figure S4 and Table S5 and S6 (Supporting Information), pDPP5T-2:PyF5 and pDPP5T-2:FAP1 solar cells exhibit comparable photovoltaic performance to the pDPP5T-2:PCBM control devices. Again, given that both fullerenes are monosubstituted, impressively high $V_{OC}$ values of 0.70 and 0.71 V were achieved for the low bandgap polymer donor in combination with PyF5 and FAP1, respectively. The performance of solar cells based on the two novel fullerene acceptors remained ≈100% after baking at 140 °C for 24 h, while the PCBM-based solar cells maintained only 31% of initial PCE under the same conditions.

The surface morphology of BHJ thin films is studied by optical microscopy (**Figure 3**), measurement of water contact angle (Figure 3, inset and Figure S5 (Supporting Information): pristine films), and atomic force microscopy (Figure S6, Supporting Information). From optical microscopy images, big crystals were formed on the surface of PTB7-Th:PCBM film after annealing at 140 °C for 0.5 h. Strong phase separation was observed for the 2 h annealed film. The contact angle of water droplet on the films were determined to be 94°, 98°, and 104° for PTB7-Th:PCBM annealed at 140 °C for 0, 0.5, and 2 h, respectively. The root mean square roughness ($R_{RMS}$) increased dramatically for PTB7-Th:PCBM BHJ films from 1.84 nm for no annealing film, to 23.3 nm for 0.5 h annealing and to 48.8 nm for 2 h annealing. For both novel fullerene-based films, no significant changes could be observed from the optical microscopy images. The contact angle of water droplet on the films as well as the $R_{RMS}$ remain almost unchanged for all the films, indicating that no phase separation or other severe morphology changes had happened to PyF5- and FAP1-based BHJ films during annealing. This underpins the relevance of the extraordinary high thermal stability observed for the corresponding photovoltaic devices.

GIWAXS measurements were performed to investigate the bulk morphology of the BHJ thin films, as shown in **Figure 4** and Figure S7 and S8 (Supporting Information). All three nonannealed BHJ films show a bimodal texture with both edge-on and face-on populations. The crystallinity of the PTB7-Th blended with FAP1 is slightly higher than that of PTB7-Th:PyF5 and PTB7-Th:PCBM blends. After 2 h annealing, the composites with PyF5 or FAP1 have slightly

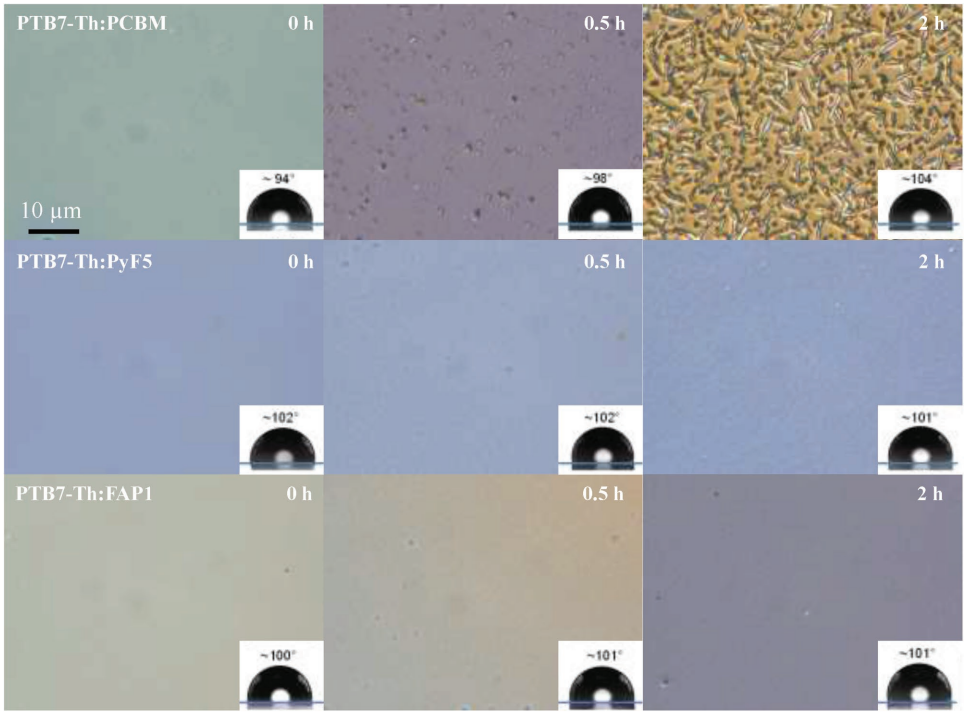


**Figure 3.** Optical microscopy images and contact angle of water droplets of PTB7-Th:PCBM films, PTB7-Th:PyF5 films, and PTB7-Th:FAP1 films.


© 2016 WILEY-VCH Verlag GmbH & Co. KGaA, Weinheim

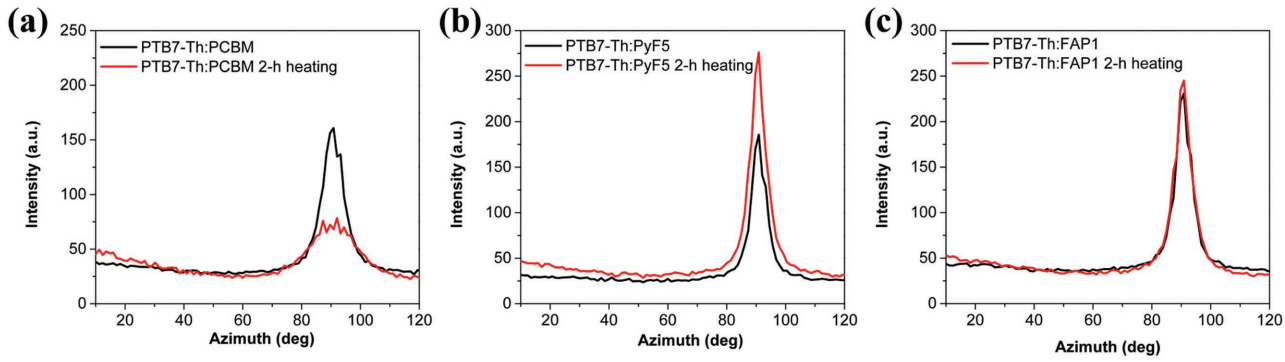


**Figure 4.** Azimuthal distribution of the polymer (100) lamellar stacking peak intensity of a) PTB7-Th:PCBM, b) PTB7-Th:PyF5, and c) PTB7-Th:FAP1 films.

enhanced intensity of (100) peak of PTB7-Th in respect to amorphous halo, whereas PTB7-Th:PCBM blend develops a different crystal mosaicity.

As depicted in Figure S9 (Supporting Information), pristine PTB7-Th displays an intense photoluminescence (PL) emission peak at 780 nm while the emission in the three nonannealed BHJ films is significantly quenched. However, the PL emission of PTB7-Th:PCBM BHJ films significantly increases after 2 h annealing, and singlet emission of PTB7-Th can be clearly distinguished, indicating a strong separation of the donor and acceptor phases. For both PTB7-Th:PyF5 and PTB7-Th:FAP1 systems, the PL spectra remain almost unchanged, which is again in excellent agreement with their extraordinary high thermal stability of BHJ solar cells. We conclude this part of the manuscript by stating that PCBM and PTB7-Th have a strong tendency to phase separate on a large scale. On the contrast, both PyF5 and FAP1 maintain their good intermixing even under thermal stress of 140 °C. This is remarkable, as both fullerenes have a comparable glass transition temperature around 100 °C. Further, FAP1 is crystalline while PyF5 is dominantly amorphous.

In order to rationalize the excellent thermal stability of PyF5- and FAP1-based solar cells, we investigated the thermodynamic properties of single components and derived the miscibility conditions in the solid–liquid equilibrium. This was done by calculating the interaction parameters between the polymer donor and the fullerene-based acceptors. The difference of the interaction energy in a mixture can be specified with the dimensionless Flory–Huggins interaction parameter ($x_{12}$). The interaction parameter is commonly used for evaluating the miscibility of organic components or of diluted solutions.[33] And it is calculated as follows[34]

$$x_{12} = \frac{v_0}{RT}(\delta_1 - \delta_2)^2 \quad (1)$$

where $v_0$ is the lattice site volume and is defined by the smallest unit; $\delta_1$ and $\delta_2$ are the Hildebrand solubility parameters of the fullerenes and the polymer, respectively; $R$ is the ideal gas constant and $T$ the temperature.

The interaction parameters between the polymers and the fullerenes are summarized in **Figure 5**a and Table S7 and S8 (Supporting Information). The detailed calculation can be found in the Supporting Information. It is important to note that the values were estimated under the same conditions and we concentrate our discussion on the relative trend given by the interaction parameters rather than on the absolute values. Besides, since the Flory interaction parameter is defined in terms of energies per site, it is proportional to the site volume $v_0$. The site volume must be specified whenever interaction parameter is discussed.[34] Here, we decide to give the value of $x_{12}$ in multiples of $v_0$ for the purpose of general comparison. The interaction parameter of PTB7-Th:PCBM is higher than that of PTB7-Th:PyF5 and PTB7-Th:FAP1, which indicates that PyF5 and FAP1 are more miscible with PTB7-Th than PCBM is. The same trend is observed for pDPP5T-2 mixtures, meaning better miscibility between pDPP5T-2 and PyF5 or FAP1 than between pDPP5T-2 and PCBM. A clear trend is observed between enhanced thermal stability and better polymer/fullerene miscibility.

The mixing behavior of polymer:fullerene composites were further experimentally analyzed by differential scanning calorimetry (DSC). The DSC curves depicted in Figure 5 are taken from their first heating runs. In Figure 5b, the melting peaks of PCBM in pristine and in blends are more or less located at the same temperature (282 °C). Cold crystallization of PCBM occurred in all the examined blends at temperatures between 140 and 160 °C. The cold crystallization enthalpy and the melting enthalpy for the pristine components as well as for the blends were calculated by integrating the peak area. For pristine PCBM, the cold crystallization at ≈160 °C accounts for only 21% of the melting enthalpy, however, for the blends, 90% of the melting enthalpy is contributed from cold crystallization. We interpret this finding that the addition of PTB7-Th to PCBM restricts the crystallization of PCBM during drying. However, upon heating, PCBM gains enough energy to rearrange and transform the aggregated but disordered regions into crystallites, resulting in cold crystallization as observed in Figure 5b. Figure 5c depicts the DSC heating curves for PyF5 and corresponding blends. Owing to the amorphous nature of PyF5, DSC does not give specific insight into the thermal behavior of pristine as well as blended PyF5. FAP1 behaves different to PCBM as well as to PyF5. The endothermic peak of pristine FAP1 is located at 269 °C (Figure 5d). In contrast to PCBM, no cold crystallization is observed for either pristine FAP1 or PTB7-Th:FAP1 blends, indicating the absence of amorphous but aggregated pristine


© 2016 WILEY-VCH Verlag GmbH & Co. KGaA, Weinheim

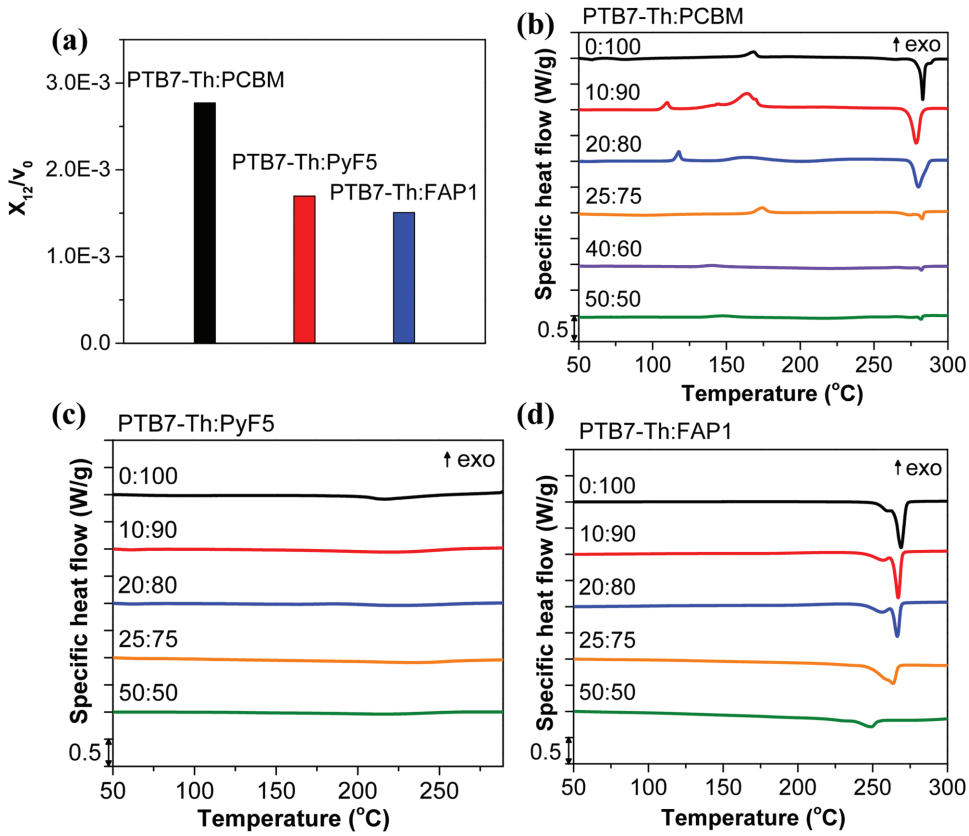


**Figure 5.** a) Interaction parameters and b–d) thermal properties of PTB7-Th:fullerene blends.

or mixed polymer:fullerene domains. Further, FAP1 shows a melting point depression upon addition of PTB7-Th, with the melting temperature being reduced to 249 °C at a mixing ratio of 50:50. The occurrence of melting point depression suggests that FAP1 forms less-perfect crystals in the presence of PTB7-Th, which is an obvious sign of chemical similarity and preferential mixing. Different from PCBM, FAP1 can still crystallize in the presence of high polymer loadings probably by forming polymer inclusions in the fullerene crystallites.

Combining the information on the interaction parameters together with the experimentally measured DSC results, we conclude that the crystallization of PCBM is hindered in the presence of PTB7-Th; a metastable solid state composite is formed under processing condition, however, PCBM has rather low miscibility with the polymer. Although entropy favors the formation of mixed aggregated regions, thermodynamics drives PCBM and PTB7-Th into phase separation. As a consequence, when sufficient energy is achieved (e.g., by heating, light excitation, etc.), PCBM is driven to phase separate from the polymer matrix, causing large scale phase separation as evidenced by the deteriorated photovoltaic performance and optical microscopy images. PyF5 is chemically more miscible with PTB7-Th due to the existence of the branched alky methoxy groups. PyF5 forms more intimately mixed phases with PTB7-Th and pDPP5T-2 than PCBM does. Moreover, unlike PCBM, PyF5 is rather amorphous and does not form ordered structure within/outside the polymer matrix. To our surprise, the semicrystalline FAP1 is also more chemically compatible with PTB7-Th and pDPP5T-2 than PCBM. In contrast to PCBM, FAP1 does not exhibit cold crystallization during heating, underpinning that the driving force for phase separation is less than PCBM. The presence of PTB7-Th does not dramatically suppress FAP1 crystallization, as the higher miscibility allows the formation of "impure" fullerene crystals, again evidencing the enhanced compatibility between these two compounds.

From our study, PyF5 and FAP1 are more miscible with PTB7-Th than PCBM, which contributes to the excellent blend film thermal stability. However, we also notice that the devices fabricated with the novel fullerene acceptors show a slightly low $J_{SC}$ and fill factor (FF). As far as we understand, the bicontinuous percolation pathways for transporting charge carriers are not easy to form when the two components have good miscibility, which leads to slightly low $J_{SC}$ and FF for OPV devices based on functional fullerene acceptors.[35] This finding shows a clear direction to the future design of novel acceptors and donors with proper miscibility and optoelectronic properties.

To summarize, we demonstrate that the low miscibility between PCBM and pDPPT5-2 or PTB7-Th is the fundamental origin of the low thermal stability. On the contrary, two novel fullerenes, PyF5 and FAP1, with a significantly higher chemical compatibility are introduced to overcome these limitations. PyF5 and FAP1 further exhibit more optimized energy levels and a higher $V_{OC}$ than PCBM does, allowing for keeping the time-zero performance losses at a minimum. Most importantly, the better chemical miscibility with PTB7-Th and pDPP5T-2 allows overcoming short-time $J_{SC}$ burn-in losses


© 2016 WILEY-VCH Verlag GmbH & Co. KGaA, Weinheim

and furthermore results in OPV devices with superior thermal stability. The combination of promising optoelectronic properties and thermal stability underlines the necessity for novel acceptor design rules balancing performance and stability. The benefit of chemical miscibility as a novel design principle for improved stability is expected to pave alternative guidelines toward designing and developing novel acceptors for efficient and thermally stable OPV devices.

## Experimental Section

*Materials*: ZnO-nanoparticle dispersion in isopropyl alcohol was from Nanograde. pDPP5T-2 (batch No.: GKS1-001) was provided by BASF. PTB7-Th was purchased from One Material. PCBM (99%) was obtained from Solenne BV. PyF5 and FAP1 were synthesized according to literature.

*Device Fabrications*: All solar cells had an inverted structure, indium tin oxide (ITO)/ZnO/active layer/$MoO_x$/Ag. The prestructured ITO coated glass substrates were subsequently cleaned in toluene, acetone, and isopropyl alcohol for 10 min each. Then, 30 nm ZnO (Nanograde, N10) was doctor bladed on the ITO substrate and annealed at 85 °C under ambient atmosphere. The PTB7-Th based active layer from chlorobenzene: 1,8- diiodooctane (100:3) solution was spin coated on top of ZnO. The pDPP5T-2 based active layer from chloroform: 1,2- dichlorobenzene (90:10) solution was processed under ambient conditions. 10 nm $MoO_x$ and 100 nm silver were deposited subsequently under $6 \times 10^{-6}$ Torr by thermal evaporation through a shadow mask to form an active area of 10.4 $mm^2$.

*Device Characterization*: The current–voltage characteristics of the solar cells were measured under AM 1.5G irradiation on an OrielSolIA Solar simulator (100 mW $cm^{-2}$). The light source was calibrated by using a silicon reference cell. All cells were tested under ambient air.

Atomic force microscopy images were obtained by using a SPM NANOEDUCATOR from NT-MDT Co. to observe the surface morphologies of the pristine films and blend films.

Film absorption was characterized with a UV–vis–NIR spectrometer Lambda 950 from PerkinElmer. Thin film photoluminescence measurements were conducted under excitation from a 375 nm diode laser. The spectra were recorded with a silicon charge-coupled device (Si-CCD) attached to iHR320 monochromator (Horiba).

DSC measurements were taken with a Q1000 from TA Instruments. The temperature ranged from 30 to 310 °C with a heating and cooling rate of 10 K $min^{-1}$. The powders (PTB7-Th, PCBM, PyF5, FAP1) were dissolved in chlorobenzene with a concentration of 2% and stirred inside the glovebox at 60 °C overnight. The solutions were mixed at the required ratios and stirred for another hour, then drop casted on clean glass substrates, and dried under inert atmosphere for 3 h and under vacuum overnight.

GIWAXS patterns of the pristine fullerenes (Figure S2, Supporting Information) were performed on the ID-10 beamline at the European Synchrotron Radiation Facilities (Grenoble, France). Diffraction patterns were collected with a Pilatus 300k detector (172 × 172 µm pixel size). The wavelength used was 1.24 Å. The measurements were performed on thin films on Si substrate at an incidence angle of 0.16°. The modulus of the scattering vector was calibrated using several diffraction order of silver behenate. In situ heating ramps were performed with Linkam heating stage. The integration of 2D-WAXS patterns was performed in a home-made routine written in Igor Pro software.

GIWAXS patterns of blend films were collected with the highly customized versatile advanced X-ray scattering instrument at the chair for Crystallography and Structural Physics (Universität Erlangen-Nürnberg, Germany). The system was equipped with a MetalJet D2 70 kV X-ray source from EXCILLUM, Sweden. The beam was shaped by a 150 mm Montel optics (INCOATEC, Geesthacht) and two of four double slit systems with the last slit system equipped with low scattering blades (JJXray/SAXSLAB). Aperture sizes were ($0.7 \times 0.7\,mm^2$, $0.4 \times 0.4\,mm^2$) for GIWAXS. The sample was located within the fully evacuated detector tube. The hybrid-pixel 2D Pilatus 300 K detector (Dectris Ltd., Baden, Switzerland) was used to collect the scattered radiation. The measurements were carried out at an energy of 9.28 keV. The collimation line was tilted and shifted with respect to the horizontal plane, allowing grazing incidence angles which maximized the scattering volume and enhanced the scattered intensity. The incidence angle $\alpha$ for GIWAXS measurements was between 0.183° and 0.189° which was smaller than the critical angle of total reflection of the glass substrate and ZnO layer to limit the penetration depth and the scattering to the thin layer. Grazing incidence geometry of the incident X-ray with respect to the sample surface was used here to enhance the scattered intensity, to maximize the scattering volume, and to access the 3D structure of the studied thin films (lateral and normal direction). The detector-to-sample distance was calibrated with a silver behenate standard to 172.6699 mm for GIWAXS. Data were reduced with Dpdak software. The samples had been probed at three different positions to check the repeatability and reproducibility of the measurements.

## Supporting Information

Supporting Information is available from the Wiley Online Library or from the author.

## Acknowledgements

C.Z. and L.K. would like to acknowledge the financial support from the China Scholarship Council (CSC). J.D.P. was funded by a doctoral fellowship grant of the Colombian Agency COLCIENCIAS, CENM. S.L. would like to acknowledge the financial support by UOS from the Bavarian State Ministry of the Environment and Consumer Protection. A.O. has to acknowledge the support of EAM Cluster. P.T., A.M., and D.K.S. acknowledge the financial support from the Russian Science Foundation (grant No. 14-13-01031). N.L. acknowledges financial support by the Bavarian Ministry of Economic Affairs and Media, Energy and Technology for the joint projects in the framework of the Helmholtz Institute Erlangen-Nürnberg for Renewable Energy (IEK-11) of Forschungszentrum Jülich. C.J.B. gratefully acknowledges the financial support through the "Aufbruch Bayern" initiative of the state of Bavaria (EnCN and solar factory of the future), the Bavarian Initiative "Solar Technologies go Hybrid" (SolTech), the SFB 953 (DFG), and the Cluster of Excellence "Engineering of Advanced Materials" (EAM), Friedrich-Alexander University Erlangen-Nürnberg.

Received: June 6, 2016
Revised: August 24, 2016
Published online: October 17, 2016

[1] a) G. Li, V. Shrotriya, J. Huang, Y. Yao, T. Moriarty, K. Emery, Y. Yang, *Nat. Mater.* **2005**, *4*, 864; b) Y. Kim, S. Cook, S. M. Tuladhar, S. A. Choulis, J. Nelson, J. R. Durrant, D. D. C. Bradley, M. Giles, I. McCulloch, C.-S. Ha, M. Ree, *Nat. Mater.* **2006**, *5*, 197; c) J. Peet, J. Y. Kim, N. E. Coates, W. L. Ma, D. Moses, A. J. Heeger, G. C. Bazan, *Nat. Mater.* **2007**, *6*, 497; d) R. Gaudiana, C. Brabec, *Nat. Photonics* **2008**, *2*, 287; e) J. You, L. Dou, K. Yoshimura, T. Kato, K. Ohya, T. Moriarty, K. Emery, C.-C. Chen, J. Gao, G. Li, Y. Yang, *Nat. Commun.* **2013**, *4*, 1446; f) Y. Liu, J. Zhao, Z. Li, C. Mu, W. Ma, H. Hu, K. Jiang, H. Lin, H. Ade, H. Yan, *Nat. Commun.* **2014**, *5*, 5293.
[2] a) S. Günes, H. Neugebauer, N. S. Sariciftci, *Chem. Rev.* **2007**, *107*, 1324; b) L. Lu, T. Zheng, Q. Wu, A. M. Schneider, D. Zhao, L. Yu, *Chem. Rev.* **2015**, *115*, 12666.

 © 2016 WILEY-VCH Verlag GmbH & Co. KGaA, Weinheim 

[3] a) G. Dennler, M. C. Scharber, C. J. Brabec, *Adv. Mater.* **2009**, *21*, 1323; b) L. Ye, S. Zhang, L. Huo, M. Zhang, J. Hou, *Acc. Chem. Res.* **2014**, *47*, 1595.
[4] J. J. M. Halls, C. A. Walsh, N. C. Greenham, E. A. Marseglia, R. H. Friend, S. C. Moratti, A. B. Holmes, *Nature* **1995**, *376*, 498.
[5] G. Yu, J. Gao, J. C. Hummelen, F. Wudl, A. J. Heeger, *Science* **1995**, *270*, 1789.
[6] J. Zhao, Y. Li, G. Yang, K. Jiang, H. Lin, H. Ade, W. Ma, H. Yan, *Nat. Energy* **2016**, *1*, 15027.
[7] S. Zhang, L. Ye, J. Hou, *Adv. Energy Mater.*, **2016**, *6*, 1502529.
[8] a) Z. He, B. Xiao, F. Liu, H. Wu, Y. Yang, S. Xiao, C. Wang, T. P. Russell, Y. Cao, *Nat. Photonics* **2015**, *9*, 174; b) P. Cheng, X. Zhan, *Mater. Horiz.* **2015**, *2*, 462; c) F. Guo, N. Li, F. W. Fecher, N. Gasparini, C. O. R. Quiroz, C. Bronnbauer, Y. Hou, V. V. Radmilović, V. R. Radmilović, E. Spiecker, *Nat. Commun.* **2015**, *6*, 7730; d) J. Zhang, Y. Zhang, J. Fang, K. Lu, Z. Wang, W. Ma, Z. Wei, *J. Am. Chem. Soc.* **2015**, *137*, 8176.
[9] N. Li, C. J. Brabec, *Energy Environ. Sci.* **2015**, *8*, 2902.
[10] W. Li, K. H. Hendriks, M. M. Wienk, R. A. Janssen, *Acc. Chem. Res.* **2016**, *49*, 78.
[11] M. C. Scharber, D. Mühlbacher, M. Koppe, P. Denk, C. Waldauf, A. J. Heeger, C. J. Brabec, *Adv. Mater.* **2006**, *18*, 789.
[12] a) E. Frankevich, Y. Maruyama, H. Ogata, *Chem. Phys. Lett.* **1993**, *214*, 39; b) C. A. Reed, R. D. Bolskar, *Chem. Rev.* **2000**, *100*, 1075.
[13] Y.-Y. Lai, Y.-J. Cheng, C.-S. Hsu, *Energy Environ. Sci.* **2014**, *7*, 1866.
[14] J. C. Hummelen, B. W. Knight, F. LePeq, F. Wudl, J. Yao, C. L. Wilkins, *J. Org. Chem.* **1995**, *60*, 532.
[15] a) H. J. Son, F. He, B. Carsten, L. Yu, *J. Mater. Chem.* **2011**, *21*, 18934; b) R. A. Janssen, J. Nelson, *Adv. Mater.* **2013**, *25*, 1847.
[16] C.-Z. Li, H.-L. Yip, A. K.-Y. Jen, *J. Mater. Chem.* **2012**, *22*, 4161.
[17] M. Lenes, G. J. A. H. Wetzelaer, F. B. Kooistra, S. C. Veenstra, J. C. Hummelen, P. W. M. Blom, *Adv. Mater.* **2008**, *20*, 2116.
[18] Y. He, H.-Y. Chen, J. Hou, Y. Li, *J. Am. Chem. Soc.* **2010**, *132*, 1377.
[19] a) M. A. Faist, S. Shoaee, S. Tuladhar, G. F. A. Dibb, S. Foster, W. Gong, T. Kirchartz, D. D. C. Bradley, J. R. Durrant, J. Nelson, *Adv. Energy Mater.* **2013**, *3*, 744; b) J.-H. Huang, Y.-S. Hsiao, E. Richard, C.-C. Chen, P. Chen, G. Li, C.-W. Chu, Y. Yang, *Appl. Phys. Lett.* **2013**, *103*, 043304.
[20] Y. Matsuo, *Chem. Lett.* **2012**, *41*, 754.
[21] K. Matsumoto, K. Hashimoto, M. Kamo, Y. Uetani, S. Hayase, M. Kawatsura, T. Itoh, *J. Mater. Chem.* **2010**, *20*, 9226.
[22] A. V. Mumyatov, F. A. Prudnov, L. N. Inasaridze, O. A. Mukhacheva, P. A. Troshin, *J. Mater. Chem. C* **2015**, *3*, 11612.
[23] M. Jørgensen, K. Norrman, S. A. Gevorgyan, T. Tromholt, B. Andreasen, F. C. Krebs, *Adv. Mater.* **2012**, *24*, 580.
[24] J. W. Rumer, I. McCulloch, *Mater. Today* **2015**, *18*, 425.
[25] a) G. Griffini, J. D. Douglas, C. Piliego, T. W. Holcombe, S. Turri, J. M. J. Fréchet, J. L. Mynar, *Adv. Mater.* **2011**, *23*, 1660; b) Z. Li, F. Wu, H. Lv, D. Yang, Z. Chen, X. Zhao, X. Yang, *Adv. Mater.* **2015**, *27*, 6999.
[26] a) Q. Tai, J. Li, Z. Liu, Z. Sun, X. Zhao, F. Yan, *J. Mater. Chem.* **2011**, *21*, 6848; b) M.-H. Liao, C.-E. Tsai, Y.-Y. Lai, F.-Y. Cao, J.-S. Wu, C.-L. Wang, C.-S. Hsu, I. Liau, Y.-J. Cheng, *Adv. Funct. Mater.* **2014**, *24*, 1418.
[27] Y. J. Cheng, C. H. Hsieh, P. J. Li, C. S. Hsu, *Adv. Funct. Mater.* **2011**, *21*, 1723.
[28] a) Z. Li, H. C. Wong, Z. Huang, H. Zhong, C. H. Tan, W. C. Tsoi, J. S. Kim, J. R. Durrant, J. T. Cabral, *Nat. Commun.* **2013**, *4*, 2227; b) H. C. Wong, Z. Li, C. H. Tan, H. Zhong, Z. Huang, H. Bronstein, I. McCulloch, J. T. Cabral, J. R. Durrant, *ACS Nano* **2014**, *8*, 1297.
[29] a) A. Distler, T. Sauermann, H.-J. Egelhaaf, S. Rodman, D. Waller, K.-S. Cheon, M. Lee, D. M. Guldi, *Adv. Energy Mater.* **2014**, *4*, 1300693; b) T. Heumueller, W. R. Mateker, A. Distler, U. F. Fritze, R. Cheacharoen, W. H. Nguyen, M. Biele, M. Salvador, M. von Delius, H.-J. Egelhaaf, M. D. McGehee, C. J. Brabec, *Energy Environ. Sci.* **2016**, *9*, 247.
[30] L. Derue, O. Dautel, A. Tournebize, M. Drees, H. Pan, S. Berthumeyrie, B. Pavageau, E. Cloutet, S. Chambon, L. Hirsch, A. Rivaton, P. Hudhomme, A. Facchetti, G. Wantz, *Adv. Mater.* **2014**, *26*, 5831.
[31] P. Cheng, C. Yan, T. K. Lau, J. Mai, X. Lu, X. Zhan, *Adv. Mater.*, **2016**, *28*, 5822.
[32] C. Müller, T. A. M. Ferenczi, M. Campoy-Quiles, J. M. Frost, D. D. C. Bradley, P. Smith, N. Stingelin-Stutzmann, J. Nelson, *Adv. Mater.* **2008**, *20*, 3510.
[33] S. Ulum, N. Holmes, M. Barr, A. D. Kilcoyne, B. B. Gong, X. Zhou, W. Belcher, P. Dastoor, *Nano Energy* **2013**, *2*, 897.
[34] R. Colby, M. Rubinstein, *Polymer Physics*, Oxford University, New York, USA **2003**.
[35] N. D. Treat, A. Varotto, C. J. Takacs, N. Batara, M. Al-Hashimi, M. J. Heeney, A. J. Heeger, F. Wudl, C. J. Hawker, M. L. Chabinyc, *J. Am. Chem. Soc.* **2012**, *134*, 15869.


© 2016 WILEY-VCH Verlag GmbH & Co. KGaA, Weinheim